Evolution of Residual Stress, Crystal Orientation, and Texture on Preheating Weld Treatment of Low Carbon Steel ASTM A572 Grade 42

Suratno Adi Saputro[1,2*], Andoko[1], Poppy Puspitasari[1,2]

[1]*Department of Mechanical and Industrial Engineering, Universitas Negeri Malang, Indonesia*
[2]*Department of QA/QC & Mechanical, Petrokon Utama Sdn Bhd, Brunei Darussalam*
[3]*Centre of Advanced Materials for Renewable Energy, Universitas Negeri Malang, Indonesia*
**Corresponding author: akh.adhi@gmail.com*

Article history:
Received: 28 July 2023 / Received in revised form: 23 January 2024 / Accepted: 28 January 2024
Available online 15 February 2024

ABSTRACT

Preheating is one type of heat treatment on the material prior to starting the welding process by increasing the temperature of the material. It is used to reduce the cooling rate during the welding processes to minimize the risk of residual stress and cracking during welding. Besides the benefits of welding, it also has a negative impact, especially on the integrity of the material, because the heating process at high temperatures will cause residual stress, which will affect the mechanical properties, chemical composition, and microstructure of the material, especially on Heat Affected Zone (HAZ). This study aims to analyze the effect of preheating at a temperature of 200 ºC on the welding for ASTM A572 Grade 42 steel with a thickness of 40mm using the SMAW (Shielded Metal-Arch welding) method. ASTM A572 Grade 42 was used in this study with carbon content of less than 0.25%. Based on the results of measurements and analysis using the XRD method, it was found that preheating resulted in reducing the residual stress on both weld metal and HAZ areas. Preheating treatment also moved the peak diffraction to the right side, which means the heat treatment affected compressive residual stress rather than tensile residual stress. For crystal orientation, area [110] has the highest peak diffraction and highest intensity. This area also was found with smaller size crystal size and higher dislocation and microstrain. While bigger crystal size with lower dislocation and microstrain were found in the area [200]. For texture, the highest density was found in the area [200], while the weaker texture was found in the areas [110] and [211]. The texture was influenced by plastic deformation due to atomic structure and its dislocation.

***Keywords**: Crystal orientation, low carbon steel, preheating, residual stress, texture*

I. Introduction

Preheating in welding is a heat treatment carried out on the material to be welded before the welding process is started. Preheating is carried out by increasing the temperature of the parent material locally on both sides of the joint to be welded to a temperature above ambient. Preheating is used to reduce the cooling rate of the weld. In general, this process is carried out to obtain two advantages: reducing the residual stress due to welding and reducing the risk of cracking during the welding process. Residual stress is the internal stress that is locked onto a material, which persists even though all external loading forces have been removed. This voltage is the result of materials that get thermal stress, which is when the material experiences non-uniform temperature changes due to uneven heat treatment and differences in cooling rates in materials that undergo heat treatment, such as welding processes.

DOI:10.17977/um016v8i12024p015

One of the methods that is widely used to reduce the negative impact caused by the welding process is to perform preheating before starting the welding process. Several studies have been conducted regarding preheating and their effects on material properties and residual stress. In one of the studies, it was obtained that the preheating process before the welding process could affect the hardness of the carbon steel welding results. The lowest hardness is obtained in materials that do not get preheating, while the highest hardness value is obtained in materials that get heat treatment before welding [1]. In another study related to the effect of preheating, it was found that the influence of preheating on the SS400 plate made the tensile stress higher than specimens that received PWHT heat treatment because the influence of PWHT changed the structure of the material to be softer [2]. Another study concluded that the welding process of SS 316L material with a heating temperature of 100 ℃, 120 ℃, and 140 ℃ results in a significant difference in hardness [3]. The other aspect that can be seen in a material characteristic is the orientation of crystal and its texture. The orientation of the crystal affects the material properties due to the material structure undergoing plastic deformation resulting in different slips. Grain boundaries can act as both inhibitors and starting points for deformation movement, leading to anisotropic behavior around grain boundaries [4] based on the arrangement of different atoms and different directions in the crystal thus forming a different texture [5]. Texture describes the orientation of grains in a material because as many physical, mechanical, and chemical properties of single crystals vary with the direction or plane of crystallography, textured polycrystals, which contain such single-crystal combinations, will naturally have an important influence on material properties.

A further study is required to evaluate the effect of preheating to reduce the residual stress caused by welding processes for carbon steel. Carbon steel is an alloy of iron and carbon with additional elements such as Si, Mn, P, S, and Cu. This type of carbon steel is commonly used in industries such as construction, petrochemical, shipping, oil and gas industries, and other similar industrial sectors [6]. This study is intended to analyze the effect of preheating on residual stress, crystal orientation, and texture in the Shield Metal Arc Welding (SMAW) process for ASTM A572 Grade 42 material as one of low-carbon steel. The result of the study can be used as an additional reference or important information for the welding, especially related to preheating treatment in the welding process.

II. Material and Methods

1. Material

The material used in this study was low-carbon steel ASTM A572 Grade 42. ASTM A572 Grade 42 steel material or commonly referred to as ST-42 Steel, is one type of material included in low carbon steel because it has a carbon content of less than 0.25%; the complete chemical composition of this low carbon steel is shown in Table 1. This type of steel is widely used in engineering structures, piping support construction, construction steel structures, bridge structures, construction machinery, mining machinery, frame structures for vehicles, trucks, even for manufacturing pressure vessels, jackfruit etc. This is because the technical specifications of this material can meet the technical requirements needed in manufacturing these components, such as strength, ductility, toughness and also good weldability of the material.

Table 1: Chemical Composition of ASTM A572 Grade 42 Materials [7]

Grade	Carbon	Manganese	Phosphorus	Sulfur	Silicon	
	Max (%)	Max (%)	Max (%)	Max (%)	Max (%)[1]	Range (%)[2]
42 [290]	0.21	1.35[3]	0.04	0.05	0.40	0.15-0.40

Notes:
1. Plate to 40mm thickness, shapes with flange or leg thickness to 75mm inclusive, sheet piling, bars, zees and rolled tees.
2. Plates over 40mm thick and shapes with flange thickness over 75mm.
3. For each reduction of 0.01 percentage point below the specified carbon maximum, an increase of 0.06 percentage point manganese above the specified maximum is permitted, up to a maximum of 1.60 %.

Table 2: Mechanical properties of ASTM A572 Grade 42 materials [7]

Grade	Yield point, min		Tensile strength, min		Minimum elongation %	
	ksi	MPa	ksi	[MPa]	in 200mm	in 50mm
42 [290]	42	290	60	415	20	24

2. Welding Method

The welding method used in this study was SMAW, which uses an electric current that forms a current arc and webbed electrodes. In the SMAW welding method, a protective gas occurs when the membraned electrode melts, so in this process, no inert gas pressure is needed to remove the influence of oxygen or air that can cause corrosion or bubbles in the welding results. The welding process occurs because of the resistance of electric current flowing between the electrode and the welding material which causes heat to reach 3000^{o}C, thus making the electrode and the material to be welded melt. The SMAW welding method is electric arc welding using webbed electrodes (flux). The function of flux in this welding is to form a slag above the weld results which functions as a protector of the weld from air (oxygen, hydrogen, etc.) during the welding process [8].

SMAW welding is the most widely used welding process in metal fabrication due to the low cost of procuring welding equipment, flexibility, portability, and versatility. For example, SMAW welding machines can use a simple transformer with a voltage of 110 volts that can be plugged into a regular electrical outlet. Electrodes are also available from manufacturers in packages ranging from 1 lb (0.5 kg) to 50 lb (22 kg). The SMAW process is very flexible and versatile because the same SMAW welding machine can be used to create a wide variety of welded joint designs in different types and thicknesses of metal and can be used for welding in all positions [9]. The welding machine used in this study is Miller OM-233 381L, which has rated output of 400 A/ 36 VDC and Ampere range of 60 - 400 A, while the electrode used AWS A5.1.E7016.

3. X-Ray Diffraction

The residual stress testing used in this study is based on ASTM E1426 standardization using the X-Ray Diffraction (XRD) method. The device used to perform this XRD test is the MiniFlex Benchtop model which is a versatile diffraction analysis instrument that can determine crystalline phase (phase ID) and quantification, percent (%) crystallinity, crystallite size and

strain, lattice parameter, Rietveld and molecular structure. Specimens for the XRD are taken from the sample for both weld metal and HAZ areas, refer to Figure 1.

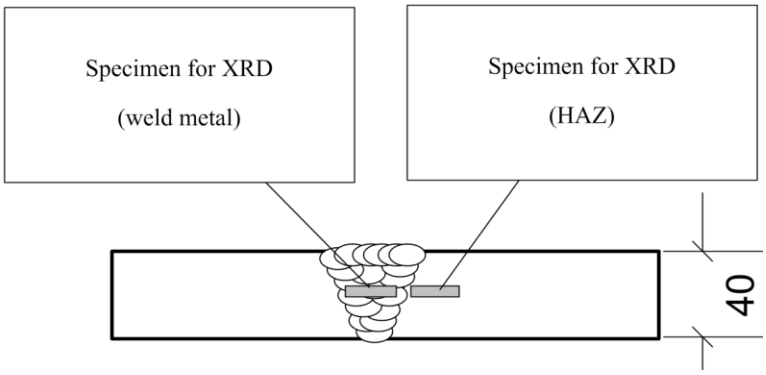

Fig. 1. Specimen for XRD for weld metal and HAZ areas

Upon completion of XRD test, the calculation of residual stress is carried out using the Bragg formula based on the value (distance) of the grid "d" determined using "d reference" (do). The "d reference" value is taken from the area that does not deform from the XRD measurement in the base metal area. Where the value of "d" hkl is obtained from Bragg's formula as shown in Eq. (1) [10]:

$$\lambda n = 2d \sin\theta \quad (1)$$

Furthermore, the strain value of the grid can be determined by the Eq (2), deviation of the grid distance d and the tension-free grid distance d_0 [10]:

$$\varepsilon = \frac{d-d_0}{d_0} = \frac{\sin\theta_0}{\sin\theta - \sin\theta_0} \quad (2)$$

After obtaining the strain value, then the residual stress value can be calculated using Eq. (3) [10] :

$$\sigma = \frac{E}{(1+v)}\left[\varepsilon_A + \frac{v}{(1-2v)}(\varepsilon_A + \varepsilon_B + \varepsilon_C)\right] \quad (3)$$

The residual stress calculation is carried out with the value of modulus of elasticity and Poisson Ratio obtained from the mechanical properties data of the base metal, with the value of (E) = 200 GPa, and Poisson (v) Ratio = 0.28. ε_A, ε_B, and ε_C are the strains measured in the corresponding directions. In this case, the strain value is using one direction as calculated in Eq. (2).

4. Crystal Orientation

The XRD is used to determine the orientation of crystals which include crystal size, microstrain, and dislocation. The crystal size is determined using the Scherrer formula which is represented as Eq. (4) [11]:

$$D = \frac{K\lambda}{\beta \cos\theta} \quad (4)$$

To determine the lattice strain value can be calculated from the Full Width at Half Maximum (β) of the diffraction peak. The relationship between particle size and lattice strain can be estimated by Eq. (5) [12]:

$$\varepsilon = \frac{\beta}{4 \tan \theta} \quad (5)$$

Meanwhile, dislocation can be calculated by Eq. (6), the length of the dislocation line per unit volume of the crystal [13]:

$$\delta = \frac{1}{D^2} \quad (6)$$

5. Texture

Texture data is obtained from the result of X-Ray Diffraction measurement which is processed using QualX software and MAUD software. The texture diffraction pattern in 2 (range 10º-90º and step size 0.0170º with X-ray source electrodes of copper metal (Cu) having a wavelength (λ) of 0.15406 Å. The texture is plotted into two parts, namely "pole figure" and "inverse pole figure" based on ND (Normal Direction), TD (Transverse Direction), and RD (Rolling Direction).

III. Result and Discussion

1. Residual Stress

The XRD measurements provided two-axis data, namely "X" which describes the angle of 2 theta and the axis "Y" which describes intensity. From the calculation of residual stress, it was found that there is a shift in diffraction patterns from the reflection of the area on each specimen. Base metal becomes a basis or reference point on this diffraction pattern as it was not affected by heat during the welding process. From the shift in the diffraction peak, it shows a change in the distance between the areas of the crystal lattice in the measurement area, which is caused by the residual stress on each material.

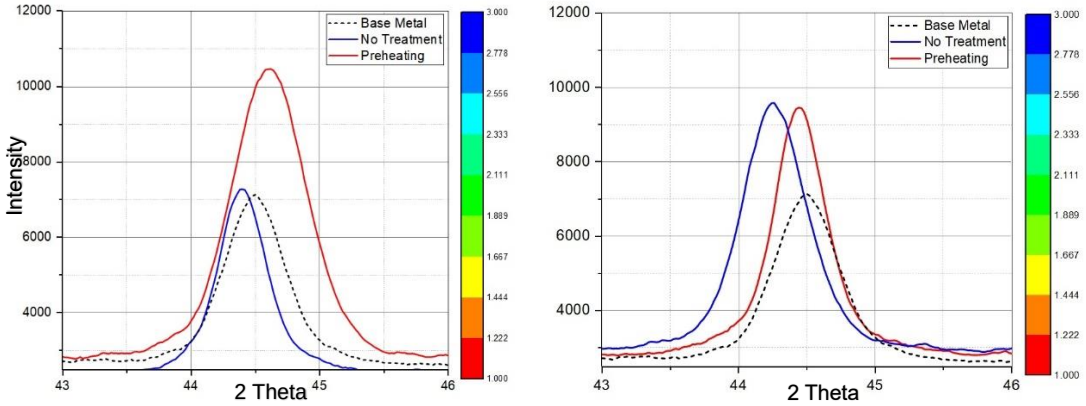

Fig. 2. Pattern of diffraction (a) HAZ (b) Weld metal

The pattern of diffraction in Figure 2 shows that there is tensile residual stress for specimens without any treatment indicated by the peaks shifted to the left. While for specimens with preheating treatment both specimens show that the patterns of diffractions are shifted to the

right. This means the preheating treatment causes compressive residual stress. In line with the pattern of diffraction in Figure 3: when the tensile residual stress is occurred, then the d spacing increases and the diffraction peak shifts to a lower angle, while when the compressive residual stress is occurred, d spacing decreases and the diffraction peak shifts to a higher angle [14]. The tensile residual stress occurs due to shrinkage when the metal is freezing; freezing starts from the side of the metal that does not melt so that the weld metal is attracted when shrinkage occurs. The presence of compressive residual stress on the surface of the material will increase resistance of the material to the stress corrosion and fatigue lives, while tensile residual stress has the opposite effect, which poses a serious threat to the performance and service life of welded materials because it triggers dimensional instability, reduces strength and various forms of failure (cracking) [15] and also reduces the resistance of material to the corrosion [16].

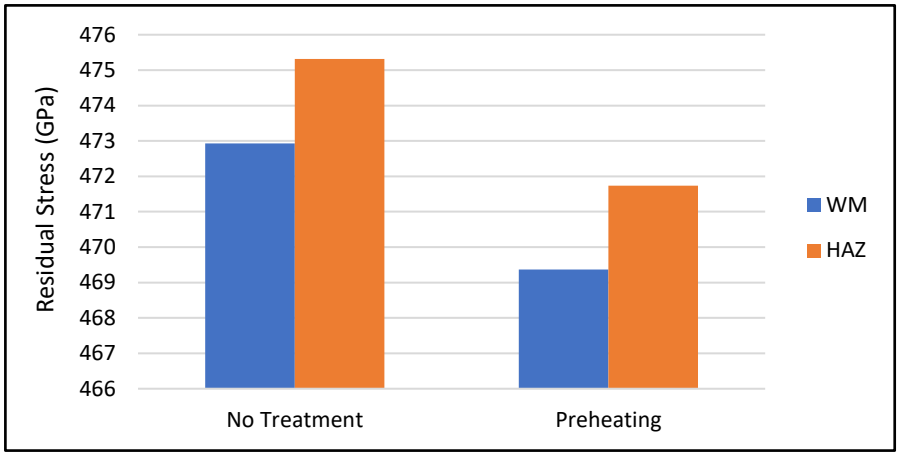

Fig. 3. Result of the residual stress calculation

Referring to Figure 3, it shows the result of the calculation for residual stress using Bragg's formula. Specimen without any treatment has a higher value of residual stress than specimen with preheating treatment before starting the welding process.

2. Crystal Orientation

Based on the result of the XRD measurement, as shown in Figure 5, it shows the 3 specimens have 3 peaks of diffraction with the area of orientation [110], [200], and [211]. Crystal orientation, including crystal size, microstrain, and dislocation, are shown in Tables 3 and 4. Referring to Table 3 and 4, it shows that all areas [110], [200], and [211] for 2 specimens have various values of crystal size, microstrain, and dislocation. The highest value of crystal size was on specimen 1 in HAZ area [211] with value of 42.285. The highest value for microstrain was also on specimen 2 on weld metal area [110], while the highest value of dislocation was on specimen 2 on weld metal area [110]. Peaks diffraction with high intensity tends to go to a smaller angle and may increase the FWHM. A smaller diffraction angle on the crystal area results in an expansion of the distance in the lattice strain [17]. Increasing lattice strain value due to the increase in crystal size and agglomeration of particles is caused by the heat during welding processes [18]. The dislocation will form a closed loop inside the crystal or surface up to the difference in slip level along the dislocation line. The greater dislocation density value will result in an atomic vacuum, which in these conditions allows defects to arise. High dislocation density occurs due to the manufacturing processes [19]. The movement of

dislocation will also encounter obstacles, forming a dislocation loop and giving rise to new dislocations continuously, causing the proliferation of dislocations.

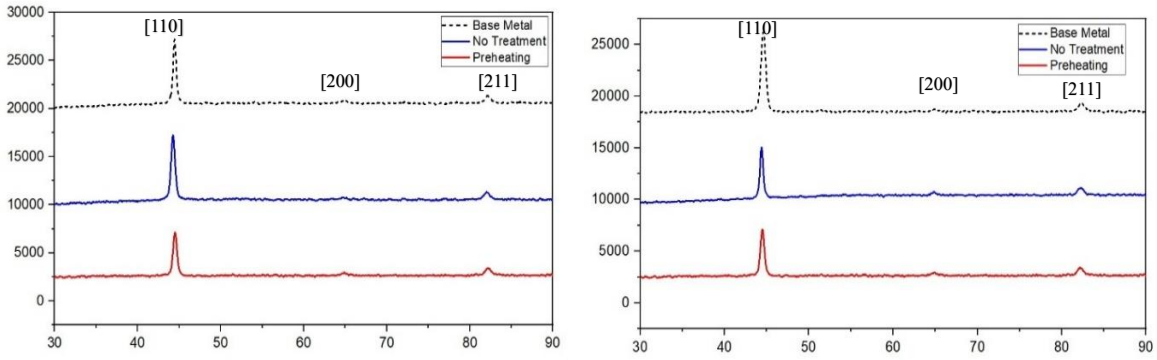

Fig. 4. Pattern of diffraction (a) Area HAZ, (b) Area weld metal

Table 3. Crystal size, microstrain, and dislocation for HAZ

Specimen	hkl	2 Theta (°)	FWHM	Crystal size (nm)	Microstrain	Dislocation
1 (No Treatment)	110	44.204	0.496	18.055	5.329	3.068
	200	64.640	0.300	32.728	2.069	0.934
	211	82.000	0.260	42.285	1.305	0.559
2 (Preheating)	110	44.401	0.351	25.532	3.753	1.534
	200	64.910	0.380	25.877	2.607	1.493
	211	82.140	0.750	14.674	3.755	4.644

Table 4. Crystal size, microstrain, and dislocation for weld metal

Specimen	hkl	2 Theta (°)	FWHM	Crystal size (nm)	Microstrain	Dislocation
1 (No Treatment)	110	44.359	0.367	24.415	3.928	1.678
	200	64.890	0.370	26.573	2.540	1.416
	211	82.178	0.310	35.513	1.551	0.793
2 (Preheating)	110	44.554	0.639	14.032	6.806	5.079
	200	64.900	0.700	14.047	4.804	5.068
	211	82.170	0.620	17.755	3.103	3.172

3. Texture Analysis

The texture is plotted from MAUD software into two parts, which are “Pole Figure” and “Inverse Pole Figure” based on ND (Normal Direction), TD (Transverse Direction), and RD (Rolling Direction). The texture for specimen 1 (no treatment) and 2 (preheating) for both HAZ and Weld Metal are shown in Figure 5.

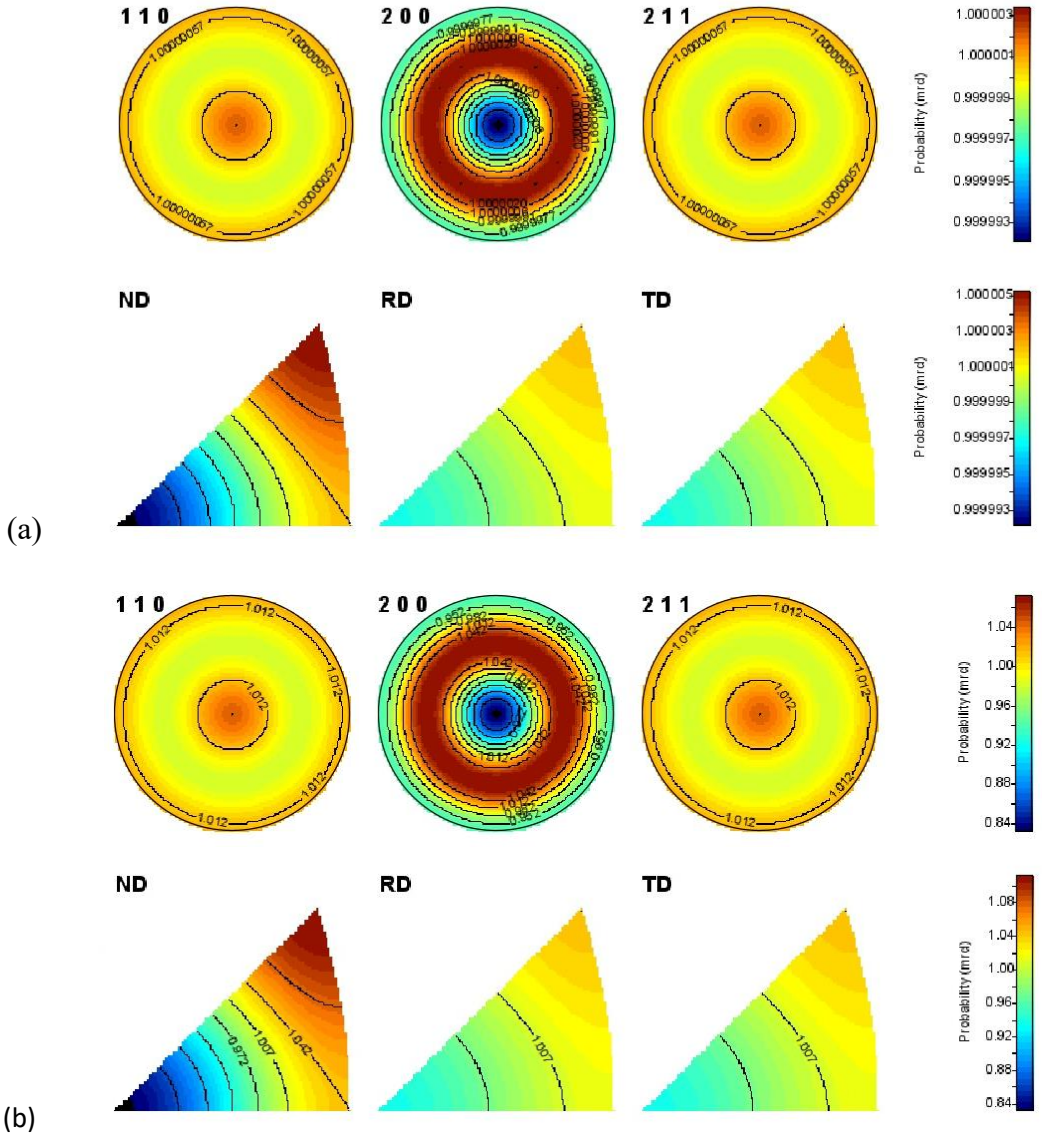

Fig. 5. Pole figure and inverse pole figure specimen 1 (a) Weld metal (b) HAZ

Figure 5 shows the distribution of crystal orientation with various values for specimen 1, which is a specimen without any treatment before and after welding processes. For the area [110] on the diffraction angle 44.20º (HAZ), 44.36 (WM), and [211] on the diffraction angle 82.00º (HAZ), 82.34º have density 1.0000057 for HAZ and 1.012 for weld metal, with crystal orientation patterns in less density. Area [200] on the diffraction angle 64.64º (HAZ) and 64.89º (WM) has density between 0.952 to 1.042 with denser on crystal orientation patterns. The crystal orientation pattern with less density may affect the vulnerable areas for cracking in the material.

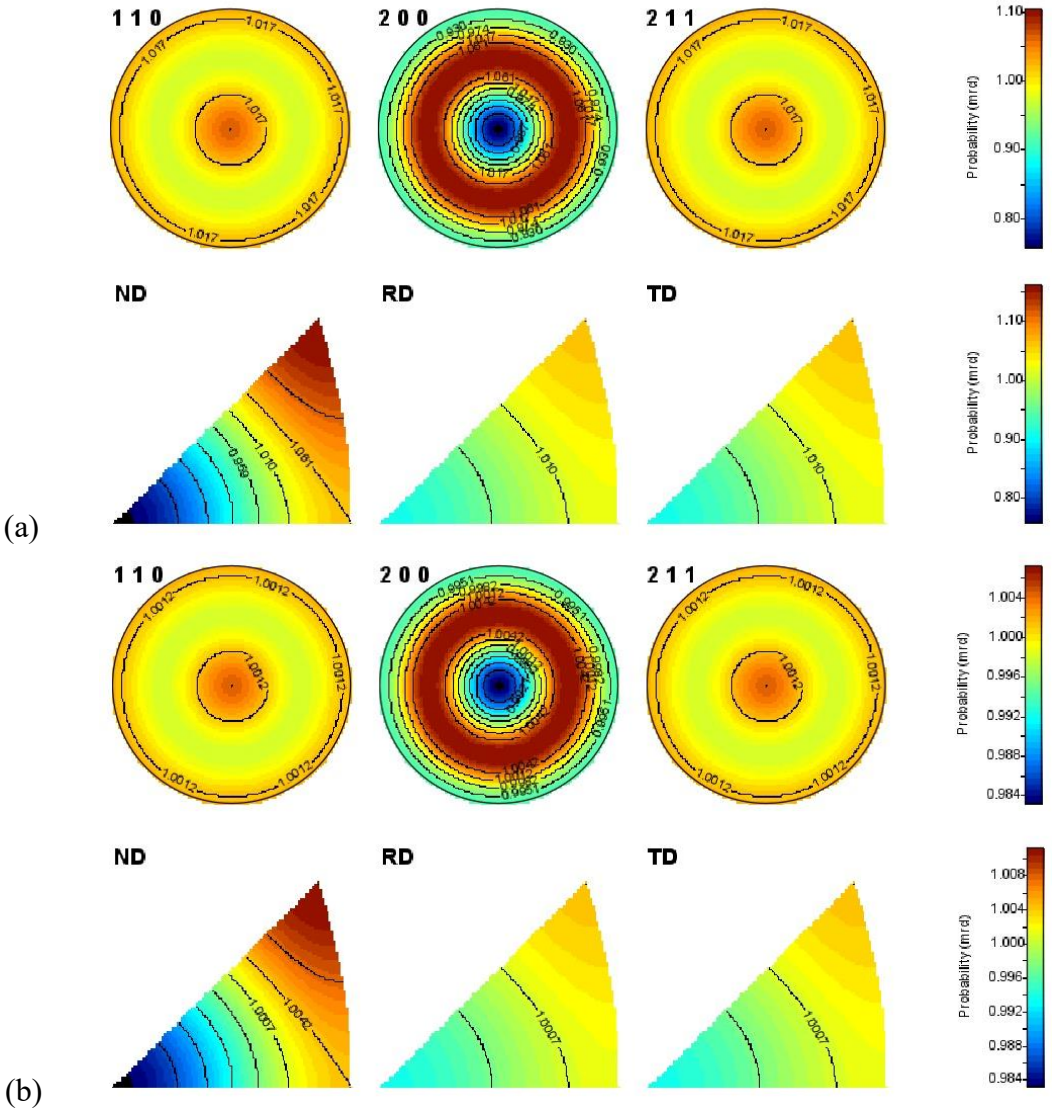

Fig. 6. Pole figure and inverse pole figure specimen 2 (a) Weld metal (b) HAZ

Figure 6 shows the distribution of crystal orientation with various values for specimen 2 which is specimen with preheating treatment prior to the welding processes. For the area [110] on the diffraction angle 44.40º (HAZ), 44.55º (WM), and [211] on the diffraction angle 82.14º (HAZ), 82.17º have density 1.017 for HAZ and 1.0012 for weld metal, with crystal orientation patterns in less density. Area [200] on the diffraction angle 64.91º (HAZ) and 64.90º (WM) has density between 0.930 to 1.061 (HAZ) and 0.9951 to 1.0042 with denser on crystal orientation patterns. The crystal orientation pattern with less density may affect the vulnerable areas for cracking in the material.

Pole figure for the area [200] shows texture movement due to plastic deformation formed because of atomic dislocation [20]. Atomic dislocation allows the material to change shape when pressure or stress is applied whereby the material will fracture or crack without damaging the basic crystal structure [21]. Furthermore, it allows the dislocation to move in the direction

of the RD (rolling direction) so that the slip line in the wave-shaped plane is difficult to identify. The area [110] and [211] have high probability to have weak texture due to sudden change in atomic structure at a low stress level and irregular crystallographic form so that it is prone to have defects [22]. This condition affects the mechanical properties of the material which include the strength and toughness of the material. The crystal probability should be controlled to maintain material integrity including its mechanical properties by controlling the processes during fabrication, construction of manufacturing of the material [23].

The comparison of density of texture for specimen 1 (no treatment) and 2 (preheating) is shown in Table 5.

Table 5. Density of the texture

hkl	Density			
	Specimen 1 (no treatment)		Specimen 2 (Preheating)	
	WM	HAZ	WM	HAZ
[110]	1.012	1.0000057	1.0012	1.017
[200]	0.9999 – 1.000	0.952 to 1.042	0.9951 to 1.0042	0.930 to 1.061
[211]	1.012	1.0000057	1.0012	1.017

Normal direction (ND) is the through-thickness direction where the mechanical properties of the material are different from rolling direction (RD) and transverse direction (RD) [24]. Normal direction (ND) indicates an increase in intensity and the poles are evenly distributed so that they experience texture deformation and the presence of high stress that occurs at the grain boundary which can eliminate mechanical anisotropy [25]. Rolling direction (RD) and transverse direction (RD) have a relatively low polar density distribution and a small texture that undergoes plastic deformation so that it has anisotropy properties that affect yield strength [26]. The properties of anisotropy will affect material properties such as elasticity, yield strength, electrical conductivity, piezoelectricity, magnetic susceptibility, light refraction, and wave propagation [27].

IV. Conclusions

Residual stress as part impacts of the welding process for low carbon steel ASTM A572 Grade 42 can be reduced by providing heat treatment before begins the welding process. Preheating prior to starting the welding processes resulted in reducing the residual stress. Furthermore, preheating treatment also shifted the peak diffraction to the right side which means the heat treatment effecting compressive residual stress rather than tensile residual stress. For crystal orientation, the highest peak diffraction was found in the area [110] with the highest intensity. However, the area [200] averagely has a bigger crystal size and lower microstrain and dislocation. While the area [110] averagely has a smaller crystal size and higher microstrain and dislocation on both HAZ and weld metal areas. Among these 2 variants, specimen 1 has the biggest crystal size in HAZ area [211] with value of 42.285. The highest value for microstrain was also on specimen 2 on weld metal area [110], while the highest value of dislocation was on specimen 2 on weld metal area [110]. For texture, the area [200] in all specimens for both weld metal and HAZ areas shows the textures with the highest density due to plastic deformation

occurs due to atomic dislocation. While areas [110] and [211] have weaker texture due to the sudden change in atomic structure at a low-stress level and irregular crystallographic so that it is prone to defects. To have more comprehensive data on the effectiveness of preheating in reducing the residual stress and its effect on the crystal orientation and texture, a further study may be required with variants in temperature and duration of preheating. The sample of study may be chosen from different types of low carbon steel.

V. Acknowledgement

The authors would like to thank Universitas Negeri Malang for the opportunity, support and guidance provided during the study of this work.

References

[1] M. Nafi, D. Sulistyono, I. Wahid, and A. U. Albab, "Analisis pengaruh preheating terhadap hasil pengelasan SMAW pada ASTM A53 dengan variasi temperature dan waktu dengan pengujian kekerasan dan struktur mikro," *Mekanika: Jurnal Teknik Mesin*, vol. 7, no. 2, 2022.

[2] R. S. P. Dora, "Analisa kekuatan material SS400 dengan pengaruh preheat dan PWHT dengan menggunakan metode simulasi dan uji tarik," Fakultas Teknologi Kelautan - ITS, Surabaya, 2012.

[3] D. L. Edy and I. Sujono, "Hardness evaluation on SS 316L joined with gas tungsten arc welding under constant heat treatment," *Journal of Mechanical Engineering Science and Technology*, vol. 4, no. 1, pp. 54–60, 2020, doi: 10.17977/um016v4i12020p054.

[4] Z. Wang, J. Zhang, and J. Lu, "Effects of crystallographic orientations and grain boundaries on nanoscratching behaviour of unique bi-crystal Cu," *Wear*, vol. 498–499, p. 204313, Jun. 2022, doi: 10.1016/j.wear.2022.204313.

[5] W. Skrotzki, "Introduction to texture analysis: Macrotexture, microtexture and orientation mapping," *J Appl Crystallogr*, vol. 43, no. 4, pp. 947–947, 2010, doi: 10.1107/s0021889810014548.

[6] N. S. Syafei, D. Hidayat, B. Y. Tumbelaka, and L. K. Men, "Analisis korosi retak tegangan pada pipa baja karbon dalam larutan asam dan sweet gas," *Jurnal Teknologi Rekayasa*, vol. 3, no. 1, p. 137, 2018, doi: 10.31544/jtera.v3.i1.2018.137-144.

[7] A. A 572/A 572M – 07, "Standard specification for High-Strength Low-Alloy Columbium-Vanadium structural," pp. 1–4, 2008.

[8] E. R. Bohnart, *Welding principles and practices*, 5th ed. New York: MC Graw Hill Education, 2018.

[9] L. F. Jeffus, *Welding and metal fabrication*, 1st ed. New York, USA: Delmar, 2012.

[10] G. Totten, M. Howes, and T. Inoue, *Handbook of residual stress and deformation of steel*. Ohio, USA: ASM International, 2002.

[11] A. Bishnoi, S. Kumar, and N. Joshi, "Wide-angle X-ray diffraction (WXRD)," in *Microscopy Methods in Nanomaterials Characterization*, Elsevier, 2017, pp. 313–337. doi: 10.1016/B978-0-323-46141-2.00009-2.

[12] S. Dolabella, A. Borzì, A. Dommann, and A. Neels, "Lattice strain and defects analysis in nanostructured semiconductor materials and devices by high-resolution X-ray diffraction: Theoretical and practical aspects," *Small Methods*, vol. 6, no. 2, p. 2100932, Feb. 2022, doi: 10.1002/smtd.202100932.

[13] B. Fedelich, "Crystal plasticity models: dislocation based," in *Nickel Base Single Crystals Across Length Scales*, Elsevier, 2022, pp. 401–427. doi: 10.1016/B978-0-12-819357-0.00023-8.
[14] M. Croft, V. Shukla, E. K. Akdoğan, N. Jisrawi *et al.*, "In situ strain profiling of elastoplastic bending in Ti–6Al–4V alloy by synchrotron energy dispersive x-ray diffraction," *J Appl Phys*, vol. 105, no. 9, p. 093505, May 2009, doi: 10.1063/1.3122029.
[15] A. Tognan, L. Sandnes, G. Totis, M. Sortino, F. Berto, Ø. Grong, and E. Salvati, "Evaluation and origin of residual stress in hybrid metal and extrusion bonding and comparison with friction stir welding," *Int J Mech Sci*, vol. 218, p. 107089, Mar. 2022, doi: 10.1016/j.ijmecsci.2022.107089.
[16] L. Wang, Y. Lu, H. Chai, G. Huang, X. Fu, X. Cao, H. Zhang, H. Wang, and M. Vedani, "Effect of residual tensile stress and crystallographic structure on corrosion behavior of AZ31 Mg alloy rolled sheets," *Mater Today Commun*, vol. 32, p. 104065, Aug. 2022, doi: 10.1016/j.mtcomm.2022.104065.
[17] Y. Tanaka, D. Akama, N. Nakada, T. Tsuchiyama, and S. Takaki, "Effect of pearlite structure on lattice strain in ferrite estimated by the Williamson-Hall method," *ISIJ International*, vol. 55, no. 11, pp. 2515–2517, 2015, doi: 10.2355/isijinternational.ISIJINT-2015-407.
[18] M. T. Masoudi, A. Saidi, M. Hashim, and A. Hajalilou, "Comparison of structure and magnetic properties of Mn–Zn ferrite mechanochemically synthesized under argon and oxygen atmospheres," *Can J Phys*, vol. 93, no. 10, pp. 1168–1173, Oct. 2015, doi: 10.1139/cjp-2015-0014.
[19] F. R. N. Nabarro, "Electrons, neutrons and protons in engineering," in *Theory of crystal dislocations*, Oxford, UK: Clarendon Press, 1967.
[20] W. Pang, K. Xin, A. Liu, R. Chen, and S. Yu, "The effect of interface orientation on deformation behavior of Cu/Al multilayer during tensile process," *Mater Today Commun*, vol. 34, p. 105133, Mar. 2023, doi: 10.1016/j.mtcomm.2022.105133.
[21] R. E. Smallman and A. H. W. Ngan, "Crystal defects," in *Physical Metallurgy and Advanced Materials Engineering*, Elsevier, 2007, pp. 95–160. doi: 10.1016/B978-075066906-1/50006-8.
[22] C. Xie, Z. Liu, X. He, X. Wang, and S. Qiao, "Effect of martensite–austenite constituents on impact toughness of pre-tempered MnNiMo bainitic steel," *Mater Charact*, vol. 161, p. 110139, Mar. 2020, doi: 10.1016/j.matchar.2020.110139.
[23] J.-P. Duroudier, *Crystallization and Crystallizers*. Elsevier Ltd, 2017.
[24] Y. Meng, X. Wang, H. Zongcheng, and X. Fu, "The influence of forming directions and strain rate on dynamic shear properties of aerial aluminum alloy," *Applied Sciences (Switzerland)*, vol. 8, no. 4, 2018, doi: 10.3390/app8040520.
[25] D. K. Qi, M. X. Tang, L. Lu, F. Zhao, L. Wang, and S. N. Luo, "Macrodeformation twinning in a textured aluminum alloy via dynamic equal channel angular pressing," *J Mater Sci*, vol. 54, no. 5, pp. 4314–4324, Mar. 2019, doi: 10.1007/s10853-018-3102-x.
[26] M. Manawan *et al.*, "XRD residual stress and texture analysis on 6082T aluminum alloy," *Materials Science Forum*, vol. 1028, pp. 409–414, Apr. 2021, doi: 10.4028/www.scientific.net/MSF.1028.409.
[27] P. Zhang, Y. Xin, L. Zhang, S. Pan, and Q. Liu, "On the texture memory effect of a cross-rolled Mg-2Zn-2Gd plate after unidirectional rolling," *J Mater Sci Technol*, vol. 41, pp. 98–104, 2020, doi: 10.1016/j.jmst.2019.05.076.